NANO LETTERS

2007
Vol. 7, No. 9
2584−2589

Self-Directed Growth of AlGaAs Core–Shell Nanowires for Visible Light Applications

Chen Chen,[†] Shyemaa Shehata,[‡] Cécile Fradin,[‡] Ray LaPierre,*[,†] Christophe Couteau,[§] and Gregor Weihs[§]

Centre for Emerging Device Technologies, Department of Engineering Physics, McMaster University, Hamilton, Ontario L8S 4L7, Canada, Department of Physics and Astronomy and Department of Biochemistry and Biomedical Sciences, McMaster University, Hamilton, Ontario L8S 4M1, Canada, and Institute for Quantum Computing, University of Waterloo, 200 University Avenue West, Waterloo, Ontario N2L 3G1, Canada

Received April 13, 2007; Revised Manuscript Received June 25, 2007

ABSTRACT

$Al_{0.37}Ga_{0.63}As$ nanowires (NWs) were grown in a molecular beam epitaxy system on GaAs(111)B substrates. Micro-photoluminescence measurements and energy dispersive X-ray spectroscopy indicated a core–shell structure and Al composition gradient along the NW axis, producing a potential minimum for carrier confinement. The core–shell structure formed during growth as a consequence of the different Al and Ga adatom diffusion lengths.

Inorganic dots, tubes, and wires with nanometer dimensions exhibit electrical and optical properties that may be tuned by their size and shape.[1−3] Among these structures, semiconductor nanowires (NWs) are becoming increasingly important as building blocks in diverse applications including bipolar junction transistors and logic gates, single-electron memory devices, p−n diodes, double barrier resonant tunneling diodes,[4] and biological imaging.[5] For the most part, these NW applications have been realized only in simple material systems, such as Si, or binary III−V semiconductors, such as GaAs and InP. Reports of NWs containing multiple group III (e.g., Al, In, Ga) and/or group V elements (P, As, Sb), of interest in band gap engineered optoelectronic devices, are comparatively few. Among this class of NWs, the $Al_xGa_{1-x}As$ material system is important for anticipated applications in bioimaging, displays, solid-state lighting, and single photon sources due to the ability to adjust the band gap wavelength in the visible spectrum. In this paper, we report growth-related aspects of AlGaAs NWs that emit in the visible region (∼720 nm) at room temperature and which exhibit a core−shell structure that forms naturally as a consequence of adatom diffusion.

NWs are predominantly grown by the vapor−liquid−solid (VLS) method where metal "seed" particles (usually Au) on a substrate surface act as collectors for the adatoms supplied by the growth flux. The metal particles become supersaturated with the growth species resulting in precipitation at the metal−solid interface. Nucleation occurs preferentially under the metal particles, resulting in the one-dimensional growth of NWs. Most NWs to date have been grown using metal organic vapor phase epitaxy using metalorganic group III sources (e.g., trimethylgallium) and group V hydrides. Alternatively, NWs may be grown by chemical beam epitaxy (CBE) which uses group V precursors that are cracked on entering the growth chamber into the more reactive As_2 or As_4 molecules but still use the uncracked group III metalorganics. In contrast, our NWs were grown by VLS using gas source molecular beam epitaxy (GS-MBE) where group III species (Al and Ga) are supplied as monomers from a heated solid elemental source, and the group V species are supplied as dimers (As_2) from a hydride (AsH_3) gas cracker operating at 950 °C.[6] Hence, in the case of MOVPE or CBE, the Au acts as a site for the decomposition of gaseous precursors whereas in the case of MBE the constituent elements arrive at the substrate already decomposed. Thus, VLS growth by MBE includes substantial growth on the surface not covered by Au. This often results in the partial burial of MBE-grown NWs due to two-dimensional (2-D) film growth between the NWs, and significant radial growth

* Corresponding author. E-mail: lapierr@mcmaster.ca.
[†] Centre for Emerging Device Technologies, Department of Engineering Physics, McMaster University.
[‡] Department of Physics and Astronomy and Department of Biochemistry and Biomedical Sciences, McMaster University.
[§] Institute for Quantum Computing, University of Waterloo.

10.1021/nl070874k CCC: $37.00
Published on Web 08/16/2007

of the NWs due to uncatalyzed deposition on the NW sidewalls. However, the elemental supply and precracking of the elements in GS-MBE mean that growth can take place at relatively low V/III flux ratios (generally in the range of 1.5−2).[7] These conditions generally favor more control over NW growth, particularly in the fabrication of compound semiconductor heterostructures, as compared to MOVPE, CBE, or solution-phase synthesis methods.

The growth of NWs by GS-MBE is sustained by adatoms impinging on the substrate surface, which may diffuse in a "random walk" manner to the base of the wires, then along the wire sidewalls up to the growth interface. The adatoms will either incorporate in the crystal by diffusing along the catalyst−wire interface or continue their walk on the surface to eventually desorb or diffuse in the Au particle. Compared to MOVPE which has been applied extensively to NW growth, the growth kinetics of NWs by GS-MBE is relatively unknown and further detailed studies are required.

In the present study, substrates of GaAs(111)B were first submitted to a 20 min UV−ozone treatment, etched in a 10% buffered HF solution, and rinsed with deionized water. The samples were then transported in ambient air to an e-beam evaporation system, where a 1 nm thick film of Au was deposited. The samples with Au were then transferred in ambient air to a gas source molecular beam epitaxy (GS-MBE) growth chamber. Before the actual growth, the Au-covered substrates were heated to a temperature of 500 °C for 5 min under an As_2 flux to form Au nanoparticles on the surface. Simultaneous desorption of native oxide was enhanced by the use of an inductively coupled hydrogen plasma source. After oxide removal and Au nanoparticle formation, the temperature was set to 570 °C for NW growth. Growth of NWs occurred by initiating AsH_3 flow at 3 sccm for a V/III ratio of 2.0, waiting 30 s, then opening the Al and Ga shutter. The growth was performed with the Al/Ga beam flux ratio set to a 2-D film composition of $Al_{0.37}Ga_{0.63}As$ and growth rate of 1 μm/h, as determined by earlier thin film calibration growths on GaAs (100) surfaces. For the purpose of other studies, the wires were p-doped with Be concentration of 10^{18} cm^{-3}.

After growth, the morphology of the resulting NWs was observed by a JEOL JSM-7000F scanning electron microscope (SEM) in the secondary electron mode. NWs were removed from the substrate for further analysis in scanning transmission electron microscopy (STEM) by sonicating in methanol for 1−2 min. A small volume (~10 μL) of the methanol solution was placed onto a holey carbon support grid. After methanol evaporation, NWs were found to be dispersed onto the grid as observed by a JEOL 2010F STEM using either bright field or annular dark field detectors. Energy dispersive X-ray spectroscopy (EDS) in the STEM, provided compositional analysis of the NWs using a probe size less than 1 nm, and measuring the Al $K\alpha_1$, Ga $K\alpha_1$, As $K\alpha_1$, and Au $L\alpha_1$ X-ray transitions.

NWs in methanol solution were dispersed onto silicon substrates for micro-photoluminescence (μPL) measurements in a continuous flow helium cryostat at 10 K and at room temperature. PL excitation and collection occurred through a microscope objective with numerical aperture of 0.7, providing a spot diameter of about 1 μm. The excitation was provided by a HeNe laser at wavelength of 632 nm and power of 2.5 μW. PL was resolved by a 75 cm grating spectrometer, and detected by a liquid nitrogen cooled Si CCD camera. Polarization-dependent μPL was measured at low temperatures (10 K) by rotation of a linear polarizer placed before the spectrometer along the emission path of the NW. The polarization dependence of the spectrometer and detector was confirmed to be negligible. Hence, the measured polarization dependence was that of the NWs only.

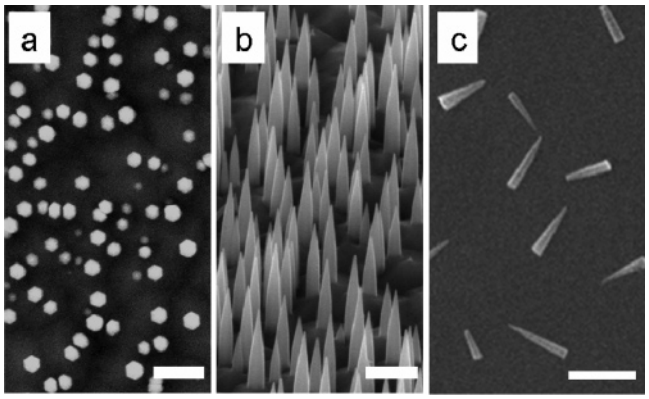

Figure 1. (a) Top view and (b) 45° tilted view of as-grown AlGaAs NWs on GaAs(111)B substrate. Scale bars are 400 nm. (c) Plan view SEM image of NWs sonicated onto a Si substrate. Scale bar is 1 μm.

Finally, fluorescent image measurements were performed on sonicated NWs deposited on glass substrates. The deposited NWs were covered with a drop of glycerol oil for confocal microscopy using a Leica TCS SP5 instrument with a Planapo 63×/1.3 NA objective. Excitation was provided by a 488 nm argon ion laser, and detection was performed using a Hamamatsu photomultiplier tube.

Panels a and b of Figure 1 show the SEM images of AlGaAs NWs as-grown on GaAs(111)B substrates and postsonicated onto silicon substrates, respectively. The AlGaAs NWs grew orthogonal to the substrate surface along the (111)B direction with the {112} family of sidewall facets as shown in the top view SEM image in Figure 1a. Electron diffraction measurements of single NWs (not shown here) confirmed that the NWs were zinc blende and grew along the (111)B direction. The AlGaAs NWs were grown for the same duration, growth conditions, and similar Au preparation method, as for GaAs NWs reported previously.[7] GaAs NWs grown from 1 nm thick Au deposits exhibited a rodlike morphology with an average diameter in the range of 20−50 nm and height of 1−2 μm. In comparison, AlGaAs NWs exhibited a more strongly tapered morphology with diameters in the range of 80−200 nm (100 nm typical) near the NW base and about 20−50 nm near the NW top, and heights of about 0.5−1 μm. This difference between AlGaAs and GaAs NW morphology can be explained by the difference in Al and Ga adatom migration lengths. NW growth occurs by diffusion of adatoms from the base to the top of NWs.[7] As NW height increases, adatom diffusion to the tops of NWs becomes increasingly unlikely and, instead of axial growth,

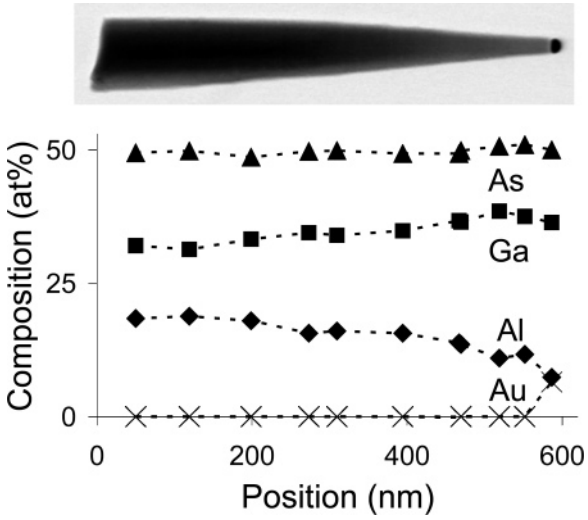

Figure 2. Bright field STEM image and EDS point measurements along the center axis of an AlGaAs NW. The Au nanoparticle is visible at the top of the NW on the right-hand side.

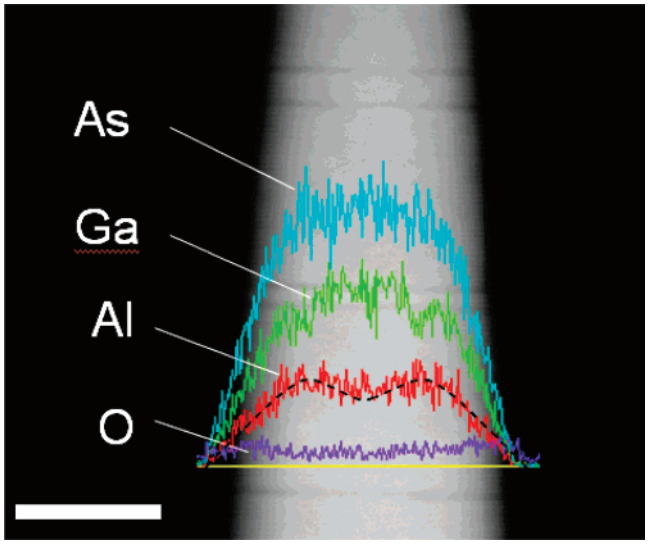

Figure 3. Annular dark field STEM image and EDS line scan across an AlGaAs NW (perpendicular to the growth direction) for the elements Al, Ga, As, and O. The dashed line on the Al line scan is a guide to the eye. Scale bar is 50 nm.

deposition occurs on the NW sidewalls. The Ga adatom diffusion length on the NW sidewall facets have not been measured directly but can be estimated to be on the order of at least 1 μm based on results from (111)B and (100) surfaces.[8,9] It is well-known that Al has a higher activation energy for migration, giving a diffusion length that is at least a factor of 4 lower compared to Ga.[10] Due to the shorter adatom migration length of Al compared to Ga, sidewall deposition is more pronounced and leads to a more tapered morphology, a wider base, and a shorter height for AlGaAs as compared to GaAs NWs.

STEM and EDS measurements were carried out to determine the overall composition and spatial distribution of elements in the NWs. A number of EDS point measurements were made along several NWs. In Figure 2, a bright field STEM image is shown for a single NW measured along the [1−1 −2] zone axis. The corresponding EDS measurements indicate that the Al composition gradually declines along the NW length (and Ga composition correspondingly increases), while the As composition remains constant. Some O is also observed due to surface oxidation of the NWs. Point EDS measurements of a half dozen similar NWs indicated an As composition of 50 atomic percent (as expected for AlGaAs). The Al composition (x) was in the range of 0.26−0.39 at the center of the NW bases with an average measurement of 0.36. The broad size distribution and spacing of the Au catalysts used in this work inevitably introduce some variability in composition, morphology, and elemental distribution in the NWs. The NW composition was somewhat lower than the nominal composition of $x = 0.37$ expected from thin film calibration growths that were performed on (100) surfaces. Similar observations have been reported elsewhere for AlGaAs NWs on GaAs substrates.[11] This difference in composition between NWs and 2-D films can be ascribed to differences between VLS and 2-D film growth mechanisms. A lower composition is expected in NWs where growth is dependent upon the diffusive transport of adatoms along the NW sidewalls toward the Au−NW interface.[12]

Compared to the base of the NWs, the Al composition at the top of the NWs (below the Au particle) was determined by EDS to be in the range of $x = 0.20-0.23$ for the half dozen NWs examined. As the NW height increases, the Al composition evidently declines (and Ga composition correspondingly increases). This can be attributed to the limited Al adatom diffusion length already described in the context of NW morphology. Again, as the NW height begins to exceed the adatom migration length, sidewall growth begins to dominate as compared to axial growth. This effect is greatest for adatoms with the shortest diffusion length, so that an accumulation of Al would be expected around the outside of the NW. To confirm this supposition, radial EDS measurements were performed across the base regions of numerous NWs (perpendicular to the growth direction). Figure 3 shows an annular dark field STEM image along the [1−1−2] zone axis, and a radial EDS line scan across the NW. Contrast lines, intersecting the NW (perpendicular to the growth direction) in the STEM image indicate the presence of stacking faults, commonly observed in (111)B oriented NWs.[13,14] These stacking faults will not be considered here. The EDS line scan reveals the anticipated core−shell structure with higher Al concentration near the outside of the NW. To confirm the core−shell structure, the line scan measurements were verified by EDS point measurements across a half dozen similar NWs. A line scan measurement across the base of the NW shows an average Al content (x) of about 0.36−0.47 at the EDS maxima near the NW edge, and about 0.26−0.39 at the NW center. Taking account of the fact that the EDS from the center is an average of the core and the shell, we estimated an increase in Al composition in the NW shell compared to the core in the range of $\Delta x = 0.023-0.044$, or 0.033 on average. With the

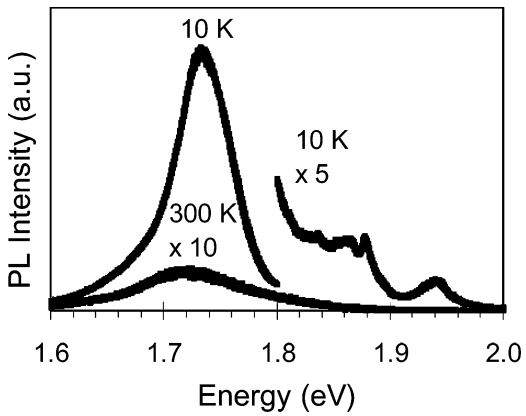

Figure 4. μPL spectra at 10 K and at room temperature (300 K) for an AlGaAs NW. The 10 K spectrum above 1.80 eV and the room-temperature spectrum are multiplied by 5 and 10, respectively, for clarity.

known relationship between AlGaAs composition and band gap energy,[15] the core−shell structure corresponds to a confinement energy of about 46 meV near the NW base. Note that the wurtzite and zinc blende polytypism evident in Figure 3 are expected to have a band gap difference of less than 5 meV,[16] which is a comparatively negligible contribution to the confinement energy.

Other possible sources exist for the variations in AlGaAs composition. First, concentration gradients have been observed due to phase separation, for example in AlInP shells on GaAs NWs.[17] However, phase separation is unlikely to be an important influence since the miscibility gap for AlGaAs is negligible under our MBE growth conditions.[18] Second, electron channeling in the sample may cause spurious deviations in the intensities of the EDS X-ray transitions.[19] However, these effects were not observed in other ternary or binary NWs such as GaAsP characterized under identical conditions. The core−shell structure is strongly evident in AlGaAs NWs due to the shorter adatom diffusion length of Al compared to other elements (In, Ga). Furthermore, the concentration gradients are significantly weakened in AlGaAs NWs when grown at higher temperatures or lower V/III flux ratios (not reported here) where Al adatom migration is enhanced.

μPL spectra were measured at room temperature (300 K) and at 10 K on NWs dispersed onto Si substrates. SEM imaging, illustrated in Figure 1c, was used to verify that the sonication procedures produced NWs with separations greater than 1 μm on average and with insignificant bunching, as compared to the μPL excitation spot diameter of 1 μm. This indicates that only a single NW at a time was likely to be excited. Typical spectra at low temperature (10 K) and at room temperature (300 K) are shown in Figure 4. First, the low-temperature spectra revealed a high-energy peak at 1.94 eV. We start by assuming that this peak may be assigned to unresolved free, donor-bound, and/or acceptor-bound exciton transitions. According to the composition dependence of the band gap and accounting for the peak energy shift with temperature for bulk AlGaAs,[20] this peak then corresponds to an Al composition of $x = 0.30$. This composition is within the range measured by EDS for the base of the NWs. A somewhat higher intensity peak is observed at 1.877 eV with a shoulder at 1.895 eV, about 45−63 meV below the exciton-related peaks. This energy difference is consistent with band-to-acceptor and/or donor-to-acceptor transitions.[20] Lower energy peaks at 1.858, 1.835, and 1.815 eV (shoulder peak) are probably phonon replicas of the higher energy transitions.[21] Quantum confinement effects are unlikely to be a significant contributing factor to the PL results since the diameter of the NWs (~100 nm) is greater than the exciton Bohr radius estimated at 18 nm.[22] Comparable peak assignments have been made in both AlGaAs thin films[23,24] and NWs.[11]

The highest intensity peak was observed at 1.731 eV at 10 K, or 1.72 eV at room temperature. The room-temperature peak, assuming a band-to-band transition, corresponds to an average $Al_xGa_{1-x}As$ composition of $x = 0.20$. This is within the range of composition measured by EDS for the top of our NWs. The relative intensity of the PL peak at 1.731 eV (corresponding to the top of the NWs) compared to 1.940 eV (bottom of the NWs) suggests that excitons are diffusing and recombining preferentially in the potential minimum near the top of our NWs. One-dimensional exciton diffusion on the order of 1 μm has been observed in GaAs quantum wires.[25] In our case, exciton diffusion is likely driven by the potential gradient due to the Al distribution seen in Figures 2 and 3. The full width at half-maximum (fwhm) of the μPL spectra was 62 meV at 10 K and 120 meV at 300 K, significantly greater compared to the expected thermal broadening observed in thin films. These large peak widths are probably due to the compositional inhomogeneities within the NWs (i.e., the axial and radial Al gradients) that are not observed in thin films.

To further confirm that the μPL spectra were obtained from single NWs, the polarization dependence of the peak PL intensity at 10 K was measured. Figure 5 shows polarization measurements performed by rotation of a linear polarizer placed before the spectrometer along the emission path of the NW. Figure 5a shows the minimum (I_{min}) and maximum (I_{max}) PL emission determined by rotation of the polarizer where a change by a factor of 10 in peak intensity was observed. The degree of emission polarization, defined as $P = (I_{max} - I_{min})/(I_{max} + I_{min})$ at the PL peak position, was 72% for our NWs. This strong emission polarization anisotropy is caused primarily by the dielectric mismatch between the NW and its surroundings, which causes strong suppression of the component of the electric field inside and perpendicular to the NW.[26] Ruda and Shik[27] calculated that the emission from GaAs NWs should have a degree of polarization of approximately 92%. Although the polarization anisotropy of 72% for our AlGaAs NWs is lower than that for GaAs NWs, it is similar to that observed for other AlGaAs−GaAs core−shell heterostructures.[28] The measured anisotropy may depend upon the morphology and compositional gradients in the NWs.

A Leica confocal microscope was used to image the light emission from NWs deposited onto glass substrates. SEM imaging, similar to that shown in Figure 1c, confirmed that the sonication process resulted in isolated NWs and no

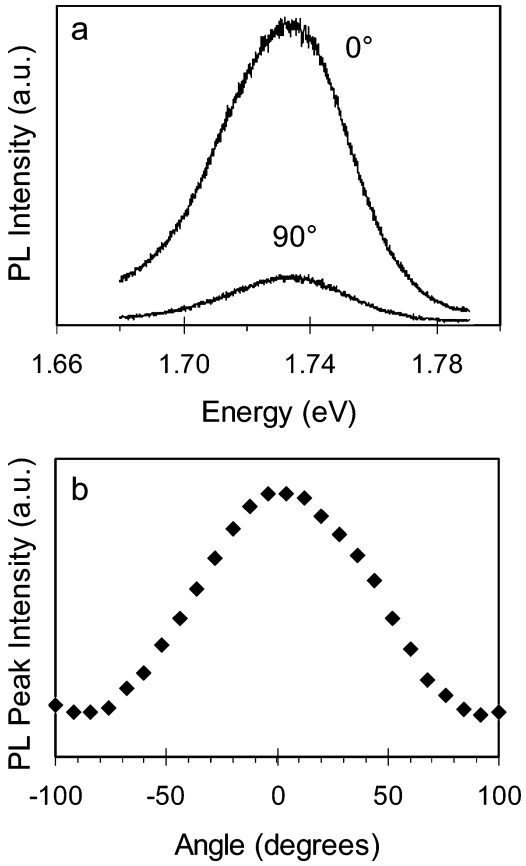

Figure 5. Polarization dependence of μPL emission at 10 K. 0 and 90° indicate the relative angle of the linear polarizer.

bunching of NWs occurred. A prism spectrometer selecting a wavelength range of 670−770 nm, placed in front of the photomultiplier tube detector, allowed only the room-temperature peak PL emission seen in Figure 4 to be detected. The spatial resolution of the confocal microscope was 139 nm in the $x-y$ plane of the substrate and 235 nm in the orthogonal z-direction, indicating that the PL emanating from one end of the wire could be resolved. The NWs lay flat on the glass substrate (as observed in SEM) and remained stationary throughout the confocal measurements, so that geometric effects associated with varying NW orientations or movement could be ruled out. Figure 6a reveals the microscopy image and Figure 6b shows the corresponding PL emission for two NWs about 1 μm in length. The PL image indicates that the emission appears to emanate near one end of the NW in support of the earlier μ-PL and EDS measurements.

In conclusion, $Al_xGa_{1-x}As$ ($x = 0.37$) NWs were grown on GaAs(111)B substrates using a gas source molecular beam epitaxy system. Strong photoluminescence polarization measured at 10 K was observed, suggesting emission from single NWs. EDS and μPL measurements indicated an Al composition gradient and a core−shell structure that apparently drove exciton diffusion to the top of NWs where recombination occurred. The core−shell structure was self-directed during growth, evolving as a consequence of the different Al and Ga adatom diffusion lengths. A complete understanding of the NW composition gradients should also consider the effect

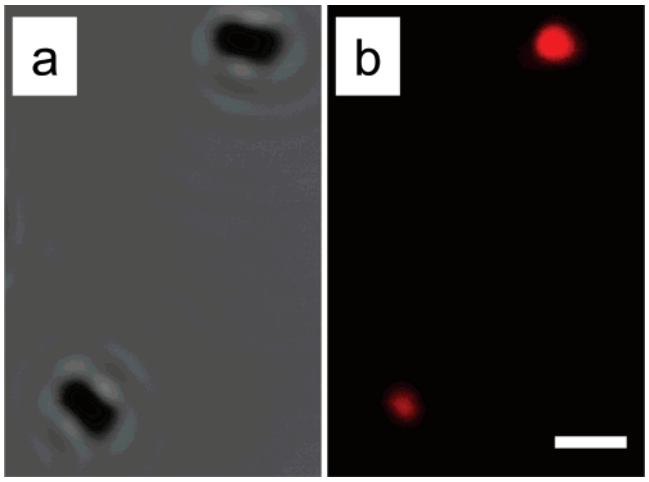

Figure 6. (a) Differential interference contrast image and (b) corresponding PL image. Scale bar is 1 μm.

of nonplanar growth associated with the NW sidewalls. For example, AlGaAs deposition on V-grooves reveals that the ternary composition is dependent on the surface orientation.[29] A quantitative understanding of the composition gradients in ternary NWs awaits further modeling of these effects.

Acknowledgment. This work was supported by a Nano Innovation grant, the Natural Sciences and Engineering Research Council of Canada, the Canadian Institute for Advanced Research, the Ontario Photonics Consortium, and the Canadian Foundation for Innovation. The authors thank Brad Robinson and the staff of the CEDT for the GS-MBE growths and the enlightening discussions, Fred Pearson and Carmen Andrei for assistance with the STEM, and Tony Collins for assistance with the confocal imaging.

References

(1) Alivisatos, A. P. *Science* **1996**, *271*, 933.
(2) Lieber, C. M. *Solid State Commun.* **1998**, *107*, 607.
(3) Smalley, R. E.; Yakobson, B. I. *Solid State Commun.* **1998**, *107*, 597.
(4) Lieber, C. M.; Wang, Z. L. *MRS Bull.* **2007**, *32*, 99.
(5) Fu, W.; Gu, B.; Boussert, K.; Koski, D.; Gerion, L.; Manna, M. L.; Gros, C. A. Larabell; Alivisatos, A. P. *Nano Lett.* **2007**, *7*, 179.
(6) Panish, M. B.; Temkin, H. *Gas Source Molecular Beam Epitaxy*; Springer Series in Materials Science 26; Springer-Verlag: Berlin, 1993.
(7) Plante, M. C.; LaPierre, R. R. *J. Cryst. Growth* **2006**, *286*, 394.
(8) Nomura, Y.; Morishita, Y.; Goto, S.; Katayama, Y.; Isu, T. *Appl. Phys. Lett.* **1994**, *64*, 1123.
(9) Shitara, T.; Kondo, E.; Nishinaga, T. *J. Cryst. Growth* **1990**, *99*, 530.
(10) Shitara, T.; Neave, J. H.; Joyce, B. A. *Appl. Phys. Lett.* **1993**, *62*, 1658.
(11) Wu, Z. H.; Sun, M.; Mei, X. Y.; Ruda, H. E. *Appl. Phys. Lett.* **2004**, *85*, 657.
(12) Johansson, J.; Karlsson, L. S.; Svensson, C. P. T.; Martensson, T.; Wacaser, B. A.; Deppert, K.; Samuelson, L.; Seifert, W. *Nat. Mater.* **2006**, *5*, 574.
(13) Bhunia, S.; Kawamura, T.; Fujikawa, S.; Nakashima, H.; Furukawa, K.; Torimitsu, K.; Watanabe, Y. *Thin Solid Films* **2004**, *464−465*, 244.
(14) Jensen, L. E.; Bjork, M. T.; Jeppesen, S.; Persson, A. I.; Ohlsson, B. J.; Samuelson, L. *Nano Lett.* **2004**, *4*, 1961.
(15) Vurgaftman; Meyer, J. R. *J. Appl. Phys.* **2001**, *89*, 5815.
(16) Akiyama, T.; Sano, K.; Nakamura, K.; Ito, T. *Jpn. J. Appl. Phys.* **2006**, *45*, L275.
(17) Skold, N.; Wagner, J. B.; Karlsson, G.; Hernan, T.; Seifert, W.; Pistol, M.-E.; Samuelson, L. *Nano Lett.* **2006**, *6*, 2743.

(18) Onabe, K. *Jpn. J. Appl. Phys.* **1982**, *21*, L323.
(19) Leifer, K.; Buffat, P. A.; Stadelmann, P. A.; Kapon, E. *Micron* **2000**, *31*, 411.
(20) Swaminathan, V.; Zilko, J. L.; Tsang, W. T.; Wagner, W. R. *J. Appl. Phys.* **1982**, *53*, 5163.
(21) Chua, S. J.; Xu, S. J.; Tang, X. H. *Solid State Commun.* **1996**, *98*, 1053.
(22) Adachi, S. *J. Appl. Phys.* **1985**, *58*, R1.
(23) Monemar, K.; Shih, K.; Pettit, G. D. *J. Appl. Phys.* **1976**, *47*, 2604.
(24) Oelgart, G.; Schwabe, R.; Heider, M.; Jacobs, B. *Semicond. Sci. Technol.* **1987**, *2*, 468.
(25) Nagamune, Y.; Watanabe, H.; Sogawa, F.; Arakawa, Y. *Appl. Phys. Lett.* **1995**, *67*, 1535.
(26) Wang, J.; Gudiksen, M. S.; Duan, X.; Cui, Y.; Lieber, C. M. *Science* **2001**, *293*, 1455.
(27) Ruda, H. E.; Shik, A. *Phys. Rev. B* **2005**, *72*, 115308.
(28) Titova, L. V.; Hoang, T. B.; Jackson, H. E.; Smith, L. M.; Yarrison-Rice, J. M.; Kim, Y.; Joyce, H. J.; Tan, H. H.; Jagadish, C. *Appl. Phys. Lett.* **2006**, *89*, 173126.
(29) Biasiol, G.; Gustafsson, A.; Liefer, K.; Kapon, E. *Phys. Rev. B* **2002**, *65*, 205306.

NL070874K